AIAA JOURNAL
Vol. 47, No. 2, February 2009

Manipulating the Flow over Spherical Protuberances in a Turbulent Boundary Layer

René Woszidlo,* Lutz Taubert,† and Israel Wygnanski‡
University of Arizona, Tucson, Arizona 85721

DOI: 10.2514/1.39930

Means of controlling the flow over a large spherical protuberance were examined. The role of suction around the base of the protuberance in reducing or even eliminating the necklace vortex created by the protuberance was considered. In the absence of suction, this vortex was lifted by the low base pressure existing behind the protuberance into the wake, thus affecting the turbulence level along its path. Large vortex generators placed upstream of the protuberance were able to delay local separation of the flow over the protuberance, thus affecting the symmetry of the wake and the level of turbulence on one side or the other. Observations made using flow visualization were supplemented by hot-wire measurements. The experiments were carried out at low speed at Reynolds numbers that did not exceed 3×10^5.

Nomenclature

A	=	area of the hemispherical obstacle perpendicular to the freestream
C_Q	=	flow coefficient, $Q/A \cdot U_\infty$
D	=	diameter of the hemispherical obstacle
d/d_1	=	width ratio of separation area
H_{12}	=	shape parameter, δ_1/δ_2
h/h_1	=	height ratio of separation area
h/h_{nv}	=	height ratio of necklace vortex
Q	=	volume flow rate
U	=	local mean flow velocity
$U_{\min}$	=	minimum mean flow velocity
U_∞	=	freestream velocity
u'	=	turbulence intensity
x	=	tunnel coordinate in direction of freestream
y	=	tunnel coordinate normal to the tunnel floor
z	=	tunnel coordinate parallel to the tunnel floor and perpendicular to the freestream
α_{sep}	=	angle between separation line and apex of hemispherical obstacle
α_{VG}	=	angle of vortex generator with respect to the freestream direction
δ	=	boundary-layer thickness
δ_1	=	displacement thickness
δ_2	=	momentum thickness
ρ	=	air density

I. Introduction

INDUSTRIAL aerodynamics fueled the interest in the flow around large protuberances that were embedded in a thick, turbulent boundary layer. Vortices shed from large buildings, silos, bridges, or stadiums were mostly investigated. Sometimes the flow around buildings was represented by simple cylindrical and spherical shapes to broaden the applicability of the results. Recently, the interest in these flows expanded to aero-optics and acoustics. The present study considers the flow around two spherical protuberances (one being a hemisphere, that is, a 180 deg segment, and the other only a 120 deg segment) embedded in a turbulent boundary layer and attempts to manipulate this flow for possible advantages in the aforementioned applications.

The prediction of the flow over surface-mounted spherical protuberances is a challenging task due to the complex three-dimensional nature of this flow. The three dimensionality causes a multifaceted interaction of separation, reattachment, and curved free shear layers that create and shed vortices of different orientations into the wake. Hawthorne and Martin [1] were among the first researchers to conduct proper experimental and theoretical investigations of the flow over a spherical segment with the intention of explaining natural phenomena like the wind blowing over a hill or patterns of water running over obstacles on river beds. Nonuniform temperature and density gradients further complicated these flows. Hawthorne and Martin [1] created theoretical models to back up their experimental observations that included vortex shedding. Baker [2] studied the flow around a cylinder and revealed a complex system of vortices evolving around its base due to the interaction of the obstacle with the oncoming boundary layer. He referred to one of them as being a "horseshoe vortex" [2], but now the term "necklace vortex" is more common. During the 1980s, major contributions to this topic were made by Toy et al. [3] and Savory and Toy [4–6], who were interested in the wind loads on hemispherical roofs and cylindrical buildings. Their results introduced two key influence parameters on the flow: the properties of the oncoming boundary layer and the Reynolds number. Savory and Toy reported that the thickness and the turbulence intensity in the boundary layer upstream of the model, with the model being fully submersed in the boundary layer, had a strong influence on the wake. Therefore, their Reynolds numbers, which are based on the freestream velocity, are not truly relevant. Because in most cases the Reynolds numbers considered were subcritical, roughening of the surfaces was necessary to simulate higher Reynolds number flows. Other investigations, concerned with vortex shedding from such obstacles and their dependence on Reynolds number, were carried out by Tamai et al. [7]. Their research focused on the number of vortex tubes forming upstream of the hemisphere and in its wake. The number of such vortex tubes and their height appeared to be closely related to the Reynolds numbers considered.

The motivation for studying the flow over a spherical protuberance changed with the development of airborne optical systems that posed different challenges than those concerning industrial aerodynamics. The ability to receive or to send a steady coherent light beam through the highly turbulent flow in the wake of the protuberance rapidly deteriorates when density variations are encountered in such a wake.

Received 21 July 2008; revision received 18 October 2008; accepted for publication 18 October 2008.

*Research Associate, Department of Aerospace and Mechanical Engineering. Member AIAA.
†Research Associate, Department of Aerospace and Mechanical Engineering. Member AIAA.
‡Professor, Department of Aerospace and Mechanical Engineering. Fellow AIAA.

This is commonly referred to as the aero-optical turret problem, resulting in aberrations that cause a reduction in the resolution, contrast, and effective range of cameras and optical sensors. Laser beams spread and scintillate, resulting in a loss of laser peak power density and a diminished accuracy of laser-guided systems. The high intensity and frequency of the turbulence in the wake of the protuberance exceed the ability of today's adaptive-optical methods to correct for the resulting aberrations. Several factors influence the aero-optical aberrations. One of them is the inclination angle of an optical beam to typical coherent structures in turbulent shear flows. Truman and Lee [8] calculated the phase distortions generated by a beam that was inclined to "hairpin-shaped" vortices. They stated that light propagation normal to the vortical structures was expected to have the least distortion. Therefore, changing the inclination angle of the vortical structures is a possible goal for flow control whose purpose is to decrease the phase distortion. Valuable contributions to the understanding of optical aberrations created by the flow over hemispherical and silo-shaped obstacles were made by Fitzgerald and Jumper [9], Gordeyev et al. [10–12], and Cress et al. [13]. They investigated the optical environment of hemispherical and cylindrical models with an embedded flat window using various measurement techniques. By applying passive control devices, they were able to change the optical properties over the flat window, but recognized that the discontinuity in the geometry due to the flat window was detrimental to the optical environment. Therefore, the application of lenses that follow the curvature was considered to be more appropriate. They also verified the dependence of the optical path difference on the freestream density and the square of the oncoming Mach number. The aforementioned difficulties inspired computational investigations of the flow over a hemisphere to verify the experimental data [14] and study a broader field of influence parameters [15–17]. Computational approaches with a variety of numerical methods turned out to be problematic, demonstrating again the complex nature of this flow.

The current investigation of the flow around a spherical protuberance is guided by several objectives. First, the usefulness of introducing streamwise vortices upstream of the protuberance had to be demonstrated. Second, the effects of large vortex generating devices in altering and shifting the wake were examined to create zones of improved aero-optical properties in the lee of the protuberance. However, it should be noted that the dependence on the various parameters has not been fully investigated as yet. Third, the application of suction along the rear portion of the base of the spherical protuberance was investigated. These approaches broaden the field of possibilities for manipulating the flow over a spherical protuberance and allow one to gain further insight into the complexity of this topic.

II. General Setup

All of the experiments were conducted in a cascade wind tunnel with a test section that is 0.61 m (2 ft) high, 1 m (3.33 ft) wide, and 2.43 m (8 ft) long. To alleviate blockage effects and provide better visual access, the sidewalls of the test section downstream of the model's location were removed during the current experiments. Because every test case was repeated multiple times to warrant repeatability, removing the side walls also allowed for quicker positioning of a camera inside the test section and for the reapplication of china clay for the surface flow visualization.

The protuberance and its height control assembly (Fig. 1a) were mounted to the bottom floor of the tunnel. The setup held a 216 mm (8.5 in.) bowling ball that was considered to be smooth. Specially machined circular base plates allowed the ball to protrude at various heights above the tunnel floor. Two configurations were considered, one being a hemisphere with an arc angle of 180 deg and the other with an arc angle of only 120 deg corresponding to half the height of the hemisphere protruding into the test section. A sleeve containing a four quadrant support structure was mounted to the bottom of the mounting plate allowing a selective application of flow control to each of the four segments of the protuberance. A threaded bar held the apparatus tightly against the tunnel floor. The top view of the setup (Fig. 1b) illustrates the position of two slots through which suction was applied. They are located at the base of the protrusion, and they formed a semicircle (extending from 90 to 270 deg from the model's leading edge) around the rear of the model. The slot was 0.8 mm (0.03 in.) wide for both heights of the protrusion.

III. Boundary-Layer Measurements

The oncoming boundary layer affected the flow over the hemisphere substantially. The effect was most visible in the recirculation area. To assess its significance, boundary-layer measurements were carried out using a hot-wire probe mounted on the centerline 200 mm upstream of the protuberance. All hot-wire

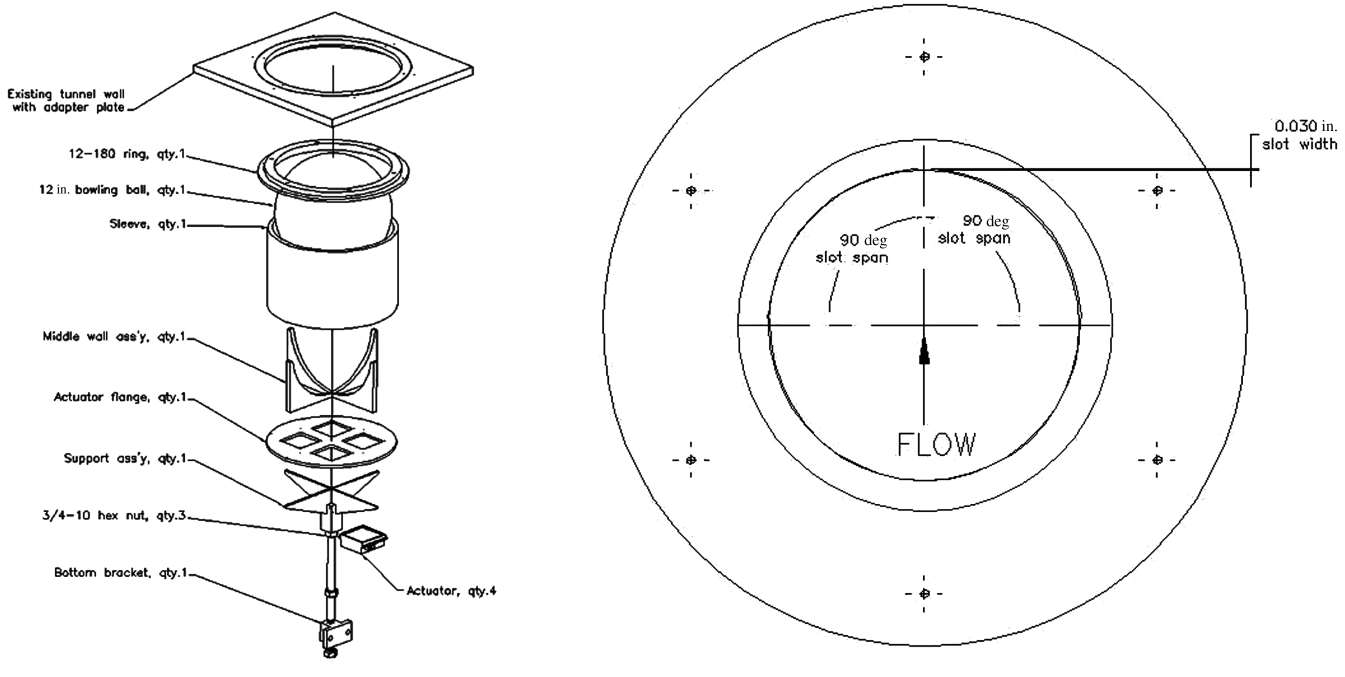

a) b)

Fig. 1 Setup in the wind tunnel and configuration of suction slots.

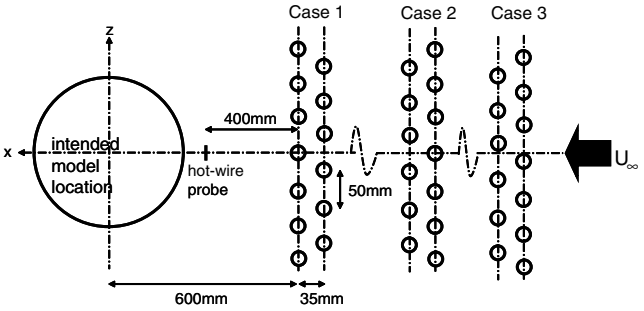

Fig. 2 Schematic view of the various nut configurations (not to scale).

measurements were performed with an AN-1003 hot-wire anemometer from A.A. Lab Systems, Ltd. The sampling rate of the hot wire was in the order of 10 kHz with a sampling time of a few seconds per data point. The hot wire was calibrated against a pitot tube with an empty test section. For the boundary-layer measurements, the model was taken out of the wind tunnel and was replaced by a solid disc that blended smoothly with the tunnel floor, thus avoiding possible interference between the model and the incoming boundary layer. Two staggered rows of hexagonal nuts, inspired by the Lego® bricks used by Toy et al. [3], spanned the tunnel floor 600 mm upstream of the intended model center location to increase the oncoming boundary-layer thickness. The nuts were 14 mm wide across the flats and protruded 8 mm from the floor. The spanwise distance between adjacent nuts was 50 mm and the distance between the rows was 35 mm. The boundary layer created by the clean tunnel floor and three different configurations of nuts, shown schematically in Fig. 2, was considered. The first case of a thickened boundary layer had a nut in the first row positioned on the centerline, the second case had a nut in the second row so positioned, and the third case had the centerline passing in between the two rows of nuts. For each case, the distance between the nuts and the planned model location remained constant. The freestream velocity U_∞ was always maintained at 20 m/s.

The boundary-layer thickness, δ, was defined as the distance from the surface at which 95% of the freestream velocity was reached. Using these data, the displacement thickness δ_1, momentum thickness δ_2, and shape factor H_{12} were computed by solving the necessary integrals numerically [18]. Table 1 lists the measured integral quantities. Compared with the baseline (clean surface boundary layer), δ_1 and δ_2 increased by more than 30% and δ increased by approximately 50%. However, the height of the spherical protuberance still exceeded the thickness of the boundary layer, leaving it greatly exposed to the freestream, in contrast to the experiments of Toy et al. [3] and Savory and Toy [4–6]. Cases 1, 2, and 3 possessed different integral values, which provided evidence for a spanwise discontinuous boundary layer. Because the nuts that were used to thicken the boundary layer also shed streamwise vortices, this spanwise inhomogeneity in the boundary-layer thickness was believed to be coherent. The measurements in [3–6] also thickened the boundary layer but were considered to be spanwise uniform, therefore neglecting an important property of the boundary layer.

Also listed in Table 1 is the factor n, which arises from the approximation of the boundary layer by a power law function: $y/\delta = (u/U_\infty)^n$. This exponent was obtained by fitting a linear function through logarithmically scaled velocity profiles.

The surface flow visualization behind the arrays of nuts is shown in Fig. 3, in which the arrows mark the streamwise vortices shed by the nuts. Essentially, each nut is a little protuberance embedded in the boundary layer forming its own necklace vortex. The footprints of the necklace vortices with the opposite sign of vorticity and originating from nuts located in different rows appeared to have merged, but what they actually did was reinforce the lifting of the fluid that was trapped between them from the surface to the edge of the boundary layer. These footprints appeared to be stable continuing downstream to the actual position of the model where they interacted with the flow around it. This interpretation of the flow visualization suggested that the location of the hot-wire probe corresponding to the configuration of case 2 should yield the thickest boundary layer (Fig. 4), whereas the configuration of case 1 should provide the thinnest one. This is indeed what transpires in Table 1. For case 3, which is probably located downstream of a vortex core, one expects that the momentum transfer across the boundary layer will be better than for case 1 (Fig. 4) but worse than for case 2. The exponent, n, also quantifies these three cases in inverse fashion; the larger this exponent is the thinner the boundary layer it represents.

Figure 5 presents the normalized velocity profiles and the associated longitudinal component, u', of the turbulence intensity. The normalized mean velocity profiles are similar but they are clearly not identical. The differences in the u' profiles are much more apparent than the differences in u. Most obvious are the differences in the distribution of u' between the baseline and all the other cases involving artificial-roughness-induced flows. The latter contain a region ($0.5 < y/\delta_1 < 3.5$) of almost constant u' resulting from the wakes created by the nuts. The turbulence intensity in this region is larger for case 2 than for the other cases due to the transport of more turbulent flow away from the wall.

Table 1 Results for δ, δ_1, δ_2, and H_{12} for the different cases

	δ, mm	δ_1, mm	δ_2, mm	H_{12}	n
Baseline	16	3.1647	2.2822	1.3867	6.6
Case 1	23	4.1891	3.2954	1.2712	7.2
Case 2	25	5.0503	3.7335	1.3527	4.5
Case 3	24	4.4974	3.3627	1.3374	4.8

IV. Experiments on the 120-Degree Spherical Segment

The application of steady suction at the trailing-edge portion of the base of the spherical segment with an arc angle of 120 deg, a boundary-layer trip at its apex, and a thickened oncoming boundary layer is discussed in this section. The freestream velocity $U_\infty = 20$ m/s, defining a Reynolds number of 250,000 based on the pedestal width of the model, corresponds to a supercritical flow. The suction was obtained by connecting a low-pressure source to the two chambers at the trailing edge of the model (see Fig. 1). The suction rate, Q, which was evenly distributed over the two chambers, was measured by a flow meter. A range of $10 < Q < 45$ scfm was applied, which corresponds to variations in $0.82\% < C_Q < 3.71\%$,

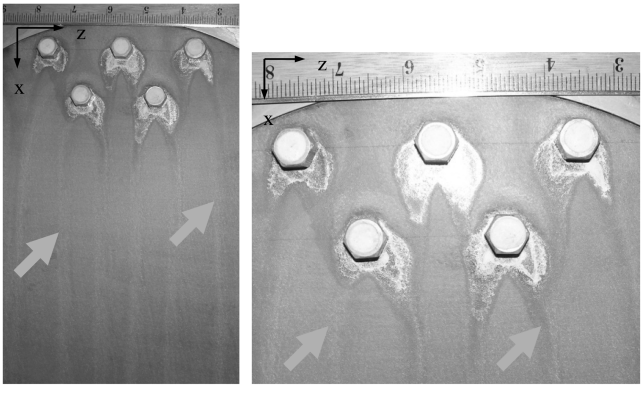

Fig. 3 Surface visualization of the flow downstream of the nuts embedded in a boundary layer.

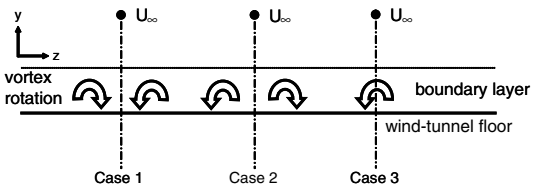

Fig. 4 Vortex rotation created by the nuts.

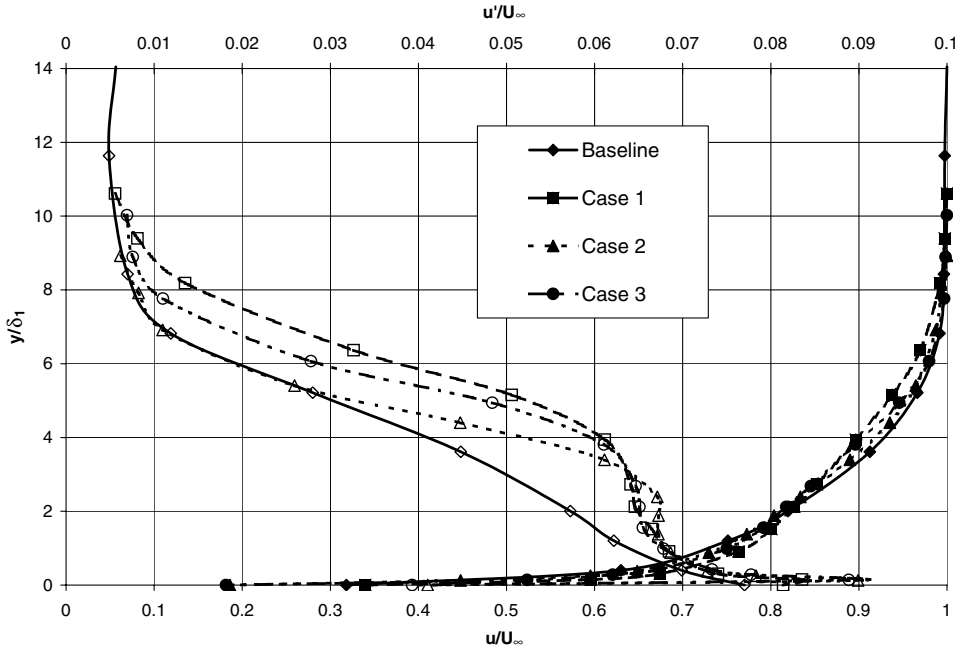

Fig. 5 Normalized boundary-layer profiles for velocity and turbulence intensity.

based on the suction rate, the freestream velocity, and the projected area of the protuberance perpendicular to the freestream direction.

The suction slot circled the azimuthal angle from 90 to 270 deg along the trailing edge of the model. This angle could be reduced at will by filling parts of the slot with clay, thereby increasing the suction velocity at a constant flow rate. The boundary layer created over the spherical segment was tripped beyond the apex of the model by a guitar string. Because of the shape of the protuberance, there was a favorable pressure gradient that resulted in a laminar boundary layer up to the apex. By tripping the boundary layer, laminar separation was averted. The thickening of the upstream boundary layer was achieved by the nut configuration of case 1, as described in the previous section. China clay, a mixture of titanium dioxide, kerosene, lighter fluid, and oleic acid, was used for surface flow visualization. Pictures were taken from both sides of the protuberance and its rear. The camera focal length and its locations were kept constant to obtain dimensionally comparable results.

Besides the visual investigation of the different cases, a hot-wire probe, using the same equipment as described for the boundary-layer measurements, was used to traverse the wake of the spherical segment. Figure 6 illustrates the setup for the measurements. The hot-wire probe traversed in the spanwise direction 1 diameter ($D = 7.36$ in. $= 187$ mm) downstream of the centerline of the protuberance and 25.4 mm (1 in.) above the tunnel floor. The incremental movement of the probe was adjusted to obtain more data points wherever large velocity gradients and strong turbulence production were expected.

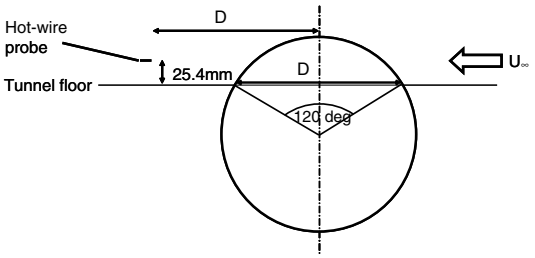

Fig. 6 Setup for hot-wire wake measurements.

A. Application of Suction, Tripping, and Thickening of the Upstream Boundary Layer

Numerous pictures were taken to obtain various quantities for the different combinations of suction, tripping the boundary layer at the apex, and alterations to the upstream boundary layer. The center high h_1 and base width d_1 of the separation region were obtained in terms of ratios to the maximum height and width of the protuberance. The ratios were obtained by a manual pixel analysis of the pictures, which had an average size of 1000×2000 pixels. All quantities measured or calculated are shown in Fig. 7.

By measuring these distances, the sizes and shapes of the separated areas were quantified to differentiate the effects for various cases. Also, the height h_{nv} reached by the necklace vortex that wrapped itself around the base of the model and was lifted into the low-pressure zone, created by flow separation, was analyzed. The visual attainment of the separation angle directly from the side view of the model was less certain and precise than the attainment of the height ratio h_1/h, which made it possible to calculate α_{sep}. The equation to calculate the separation angle, marking the location of flow separation downstream of the apex, was derived from basic geometry:

$$\alpha_{sep} = \arctan\left(\frac{\sqrt{1-(\frac{h_1}{h}(1-\cos 60\ \text{deg})+\cos 60\ \text{deg})^2}}{\frac{h_1}{h}(1-\cos 60\ \text{deg})}\right) \quad (1)$$

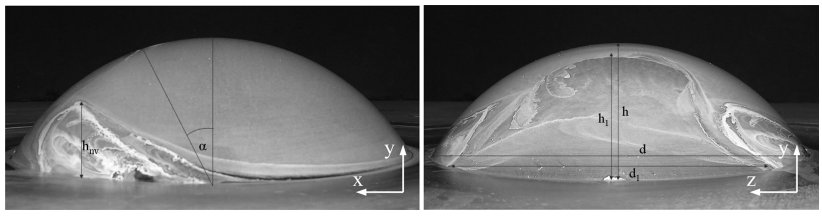

Fig. 7 Definition of quantities with the baseline flow visualization.

The application of suction through different slot spans at the rear of the model resulted in a reduction and possibly an elimination of the necklace vortex with a minimal suction rate. Starting the suction farther downstream, for example, at 120 instead of 90 deg, or ending it too early, for example, at 120 or 150 deg, caused the necklace vortex to develop again and maintain itself at a reduced intensity. Tripping the boundary layer at the apex of the model reduced the average height that the necklace vortex attained in the absence of suction. By manipulating the oncoming boundary layer and the boundary layer over the protuberance, the initial height of the necklace vortex was affected. Applying a low suction rate over the entire slot span eliminated the necklace vortex completely.

The suction also reduced the width of the separated area. However, the reduction in most of the cases was not major. The most prevalent effect occurred for the case of a thickened boundary layer combined with suction over the entire slot span, which showed a reduction of the width by up to 17%. The thickening of the boundary layer had a successful influence on the reduction of the necklace vortex.

The mentioned effects can be summarized most appropriately by the results for the separation angle, presented in Fig. 8. Applying suction over the entire slot span and manipulating the boundary layer upstream of the model caused the flow to stay attached longer and, therefore, created a smaller separated area. Note that even without suction the separation along the apex was delayed by more than 15 deg. Tripping the boundary layer at the apex of the protuberance did not have as strong an effect as the thickening of the boundary layer did. Even the combination of thickening and tripping had a lesser effect on the flow than the thickening by itself. It can be concluded, therefore, that the thickening of the boundary layer by a discrete array of nuts created streamwise vortices that had a significant effect on the flow. The trip wire seemed to eliminate the effect of these vortices by destroying or separating them. The application of suction had a small adverse effect on the separation angle because the additional downward momentum provided by the necklace vortices near the plane of symmetry disappeared with them being sucked away.

Surface visualizations photographed from the side and the rear of the protuberance of the two most diverse cases, baseline and thickened boundary layer combined with suction, are shown in Figs. 9a and 9b. respectively. By applying suction with $C_Q = 3.71\%$ and the thickening of the oncoming boundary layer, the necklace vortex was sucked away completely, the recirculation area in the rear was much smaller in height and width, and the flow separation was delayed by 26 deg compared with the baseline case. These results illustrate the influence of suction and the streamwise vortices created by the array of nuts embedded in the oncoming boundary layer.

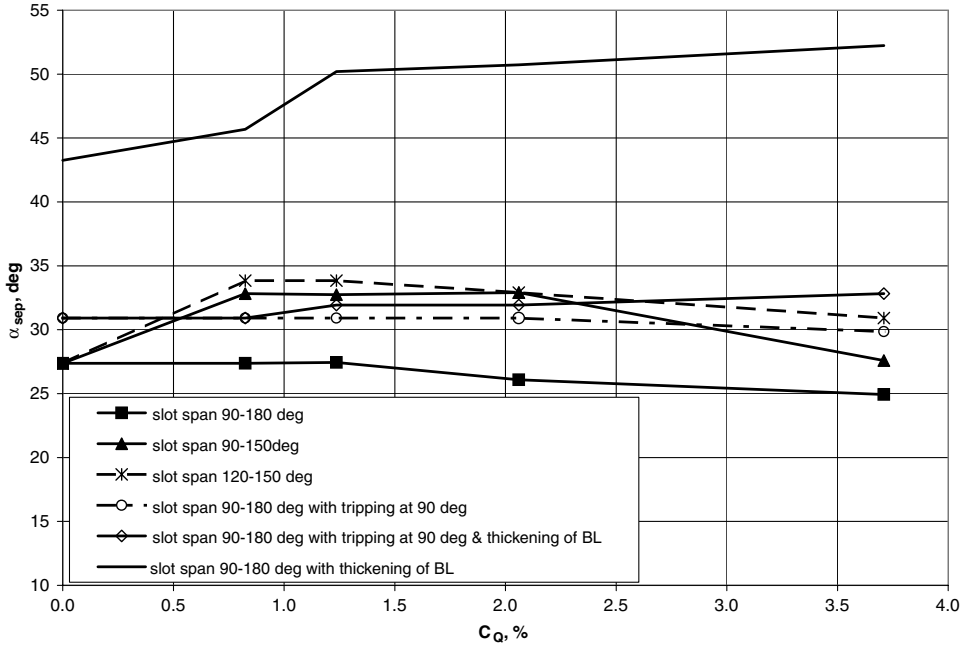

Fig. 8 Development of the separation angle α_{sep}.

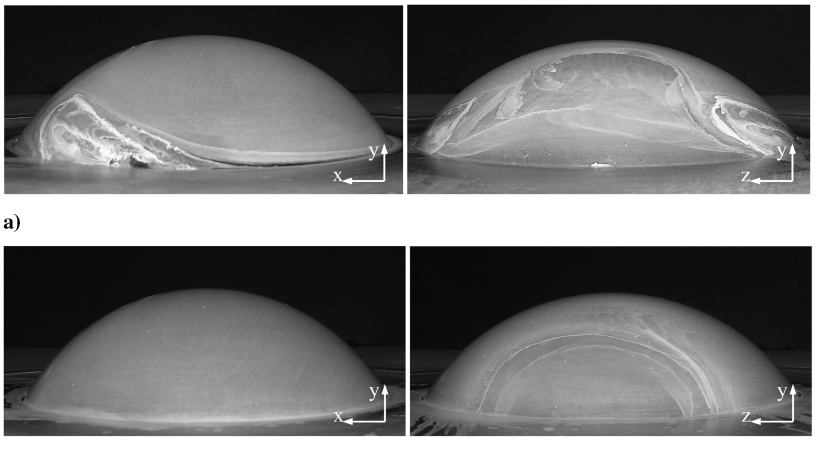

Fig. 9 Surface visualizations photographed from the side and rear of the protuberance: a) baseline (no suction, unchanged BL), and b) thickened BL with suction ($C_Q = 3.71\%$).

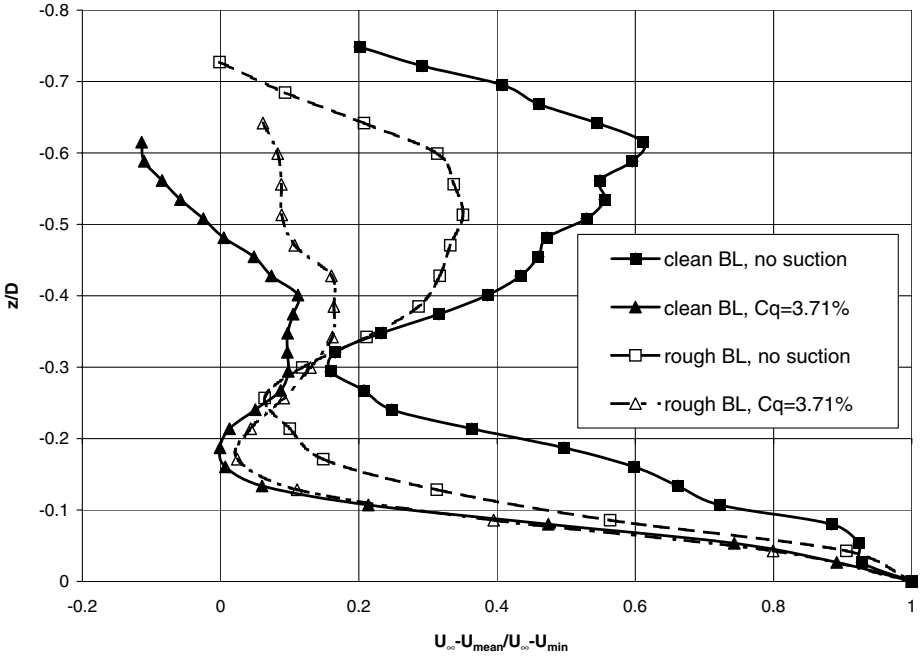

Fig. 10 Normalized wake velocity profile for a clean and rough upstream BL.

The quantitative comparison of pictures suggested in Fig. 8 revealed that various suction rates, when applied to the entire slot and a thickened upstream boundary layer, had a significant influence on the flow in the recirculation zone. Therefore, traversing the wake with a hot-wire probe was warranted. Two cases with and without the application of suction were considered, one corresponding to the natural ("clean") boundary layer and the other corresponding to a thickened one. The normalized mean velocity profiles for the four cases are shown in Fig. 10. In the absence of suction, two distinct regions of velocity deficit are observed, one near the plane of symmetry and the other, attributed to the separated necklace vortex, near the periphery of the protuberance. The nuts used to thicken the upstream boundary layer reduced this velocity defect by 30% when compared with the maximum deficit on the plane of symmetry. This implies that the strength of the necklace vortex was altered by manipulating the upstream boundary layer.

The velocity deficit identified with the necklace vortex was vastly decreased, and the location of its minimum shifted toward the plane of symmetry with the application of suction at the base of the turret. This suggests that flow separation was delayed at the sides of the spherical protuberance, concomitantly reducing the velocity defect zone near the plane of symmetry. When the suction was applied in conjunction with the clean upstream boundary layer, it even created an area where $(U_\infty - U_{\text{mean}}) < 0$, implying that the local velocity was higher than U_∞. This did not happen when the boundary layer was made thicker by using the nuts.

Similar conclusions were drawn from the normalized turbulence intensity distributions seen in Fig. 11. In the absence of suction, a second peak of high turbulence intensity can be seen downstream of the turret's periphery. Thickening the upstream boundary layer reduced the turbulence intensity of the central peak, $u'/(U_\infty - U_{\min})$, by 10% and of the side peaks by 6%; also, the high turbulence intensity region existing near the plane of symmetry shrank.

Applying suction seems to have reduced the turbulence intensity in the entire wake. The main peak of turbulence intensity became smaller and slimmer (Fig. 11) and the outer peak decreased and shifted toward the centerline, without changing the upstream boundary layer. Because the wake was traversed at one elevation, the region of maximum turbulence intensity might have not been detected because it shifted in a direction normal to the surface. Nevertheless, the changes measured are indicative of the control ability exercised by the suction and by the thickening of the upstream boundary layer. It was noted that suction did not affect the turbulence intensity as much as the thickening of the boundary layer.

B. Use of Large Vortex Generators as Passive Control Devices

The results discussed earlier imply that streamwise vortices can influence the flow over the spherical protuberance. It suggests that the flow in the lee of the model may be affected by placing large vortex generators (VGs) upstream of the protuberance. The size of the vortex generators was determined by the height of the vortex core that the VGs provided that seemed to have controlled the separation location on the model. This height was not restricted by the thickness of the boundary layer. The two possible rotations of the vortices that enhanced or opposed the evolving necklace vortex are illustrated in Fig. 12a. Looking downstream, the upper VG created a counterclockwise rotating vortex whereas the lower VG created a clockwise rotating vortex. Depending on the location of the particular VG with respect to the centerline of the protuberance, the imposed vortices either enhanced or opposed the necklace vortex surrounding the protuberance and interacted with the separation vortex.

Placing one or more VGs upstream of the protuberance, either symmetrically or not; changing their angle relative to the plane of symmetry; and combining these with a steady suction on one or both sides of the trailing edge creates a multitude of possible cases to be investigated.

The VGs had a triangular shape and were made of sheet metal. They had a maximum height of 40 mm and a length of 60 mm and were affixed to the tunnel floor 1 diameter upstream of the model's geometrical center. The VGs were inclined to the oncoming freestream at an angle of $\alpha_{\text{VG}} = \pm 25$ deg, as shown in Fig. 12. The possible VG locations are numbered to simplify the description of the various cases considered (see Fig. 12b). The VGs were located on the center line, half a radius away, or one whole radius away. This resulted in five different locations, each with two different orientations.

The results for three selected cases, listed in Table 2, are presented in the following subsections. The first case is a symmetric placement of two VGs, whereas the other two cases consider an asymmetric placement of either one or two VGs. All three cases consider an unchanged upstream boundary layer.

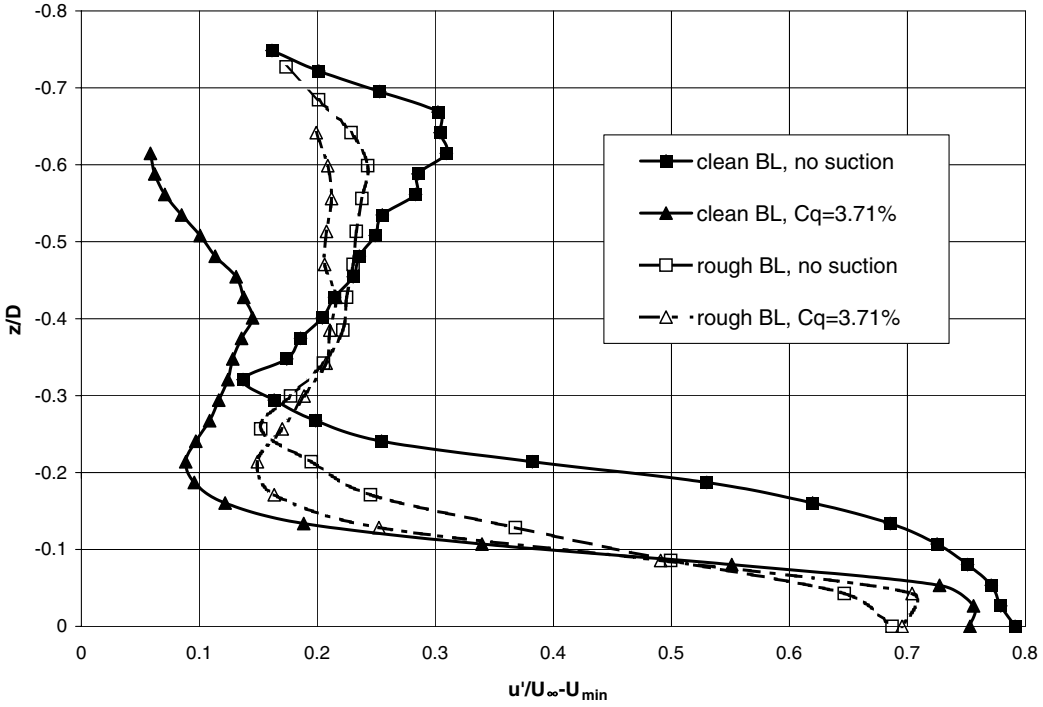

Fig. 11 Normalized wake turbulence profiles for a clean and rough upstream BL.

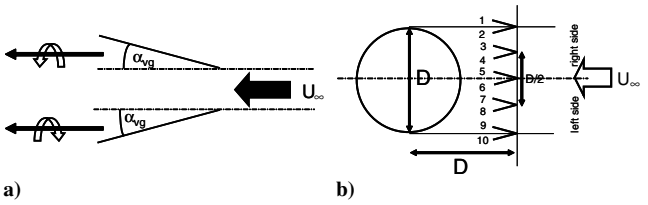

a) **b)**

Fig. 12 Velocity generators: a) vortex shedding, and b) numbered positions.

1. Case I: Large Vortex Generators in Positions 2 and 9

By placing the VGs in positions 2 and 9, two vortices were created, which rotated in the opposite direction to the necklace vortex. A comparison without suction and added suction of $C_Q = 3.71\%$, encompassing the entire slot span, is shown in Figs. 13a and 13b. The side view reveals that the height that the necklace vortex reaches is initially reduced; however, further downstream it reaches higher into the separated region than without VGs. Because of their placement and the direction of their rotation, the vortices created by the VGs caused the necklace vortex to lift up much further than it otherwise could do on its own. On the other hand, the separation of the flow at the apex of the bump was substantially delayed.

Applying suction reduced the necklace vortex, as shown in Fig. 13b. The arrows mark the visible traces of the vortices created by the VGs. The necklace vortex is not visible anymore, and the separation area is greatly decreased in comparison with the baseline case without VGs (Fig. 9). These observations are supported by hot-wire measurements of the model's wake shown in Fig. 14. The VGs shifted the maximum velocity deficit away from the plane of symmetry by creating streamwise vortices that delayed flow separation in the central region of the protuberance. Adding suction shifted the vortices created by the VGs away from the plane of symmetry, restoring the two peaks in velocity deficit (compare with Fig. 11), although the deficit in the center was still weaker.

Table 2 Considered VG configurations

	Position of VG
Case I	2 and 9
Case II	6
Case III	3 and 5

The shift in the mean velocity profiles also changed the distribution of the turbulence intensity. Without the application of suction, the highest turbulence intensity was found off the centerline, approximately corresponding to the maximum turbulence production region. Comparing the results to the baseline case without VGs (Fig. 11) reveals an overall reduction of normalized turbulence intensity of about 60%. The application of suction increased the turbulence level in the center while substantially reducing it at the sides. The aforementioned findings suggest that opposing vortices lift up the necklace vortex and, therefore, create major changes in the wake of the spherical protuberance.

2. Case II: Single Vortex Generator in Position 6

A large VG placed in position 6 created a clockwise rotating vortex, when viewed in the downstream direction, that was able to shift the wake region to the side and create a zone of vastly improved flow properties regardless of the application of suction (Fig. 15). The white arrows in Fig. 15 mark the traces of the vortex created by the VG. This vortex deflected the flow toward the left (looking downstream), delaying the separation on this side and increasing the pressure there. Therefore, the necklace vortex remained closer to the base of the protuberance, as is clearly visible in Fig. 15. The black arrows mark the separation of the flow and the vortex created by the VG. Figures 15c and 15d show the area in the rear of the model where separation is delayed. The addition of suction increased the asymmetry by keeping the flow attached a bit longer over the model.

Hot-wire measurements provided quantitative results affirming the large asymmetry in the flow. The large velocity deficit region shifted toward the right of the centerline, where the effects of the necklace vortex are visible. Suction only affected the very extreme peak of velocity deficit on the right side, and the distribution of the turbulence intensity followed suit, as shown in Fig. 16. Suction had minimal effect on the left side of the flowfield. The flow separation was greatly delayed around the centerline and the left side of the protuberance accompanied by a major reduction in turbulence intensity on that side. Again, in comparison with the results presented in Fig. 11, the normalized turbulence intensity is reduced around the centerline to one-seventh of the baseline value in the absence of the VGs.

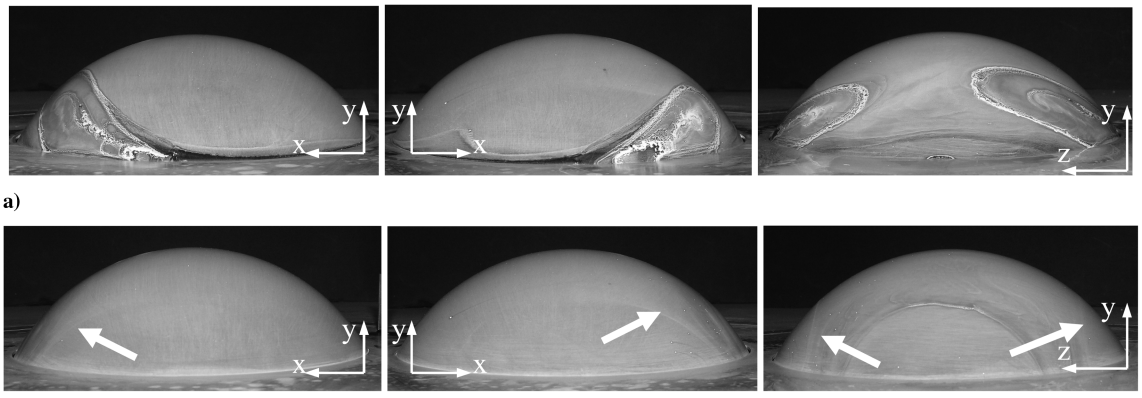

Fig. 13 VGs in positions 2 and 9: a) without suction, and b) with suction, $C_Q = 3.71\%$.

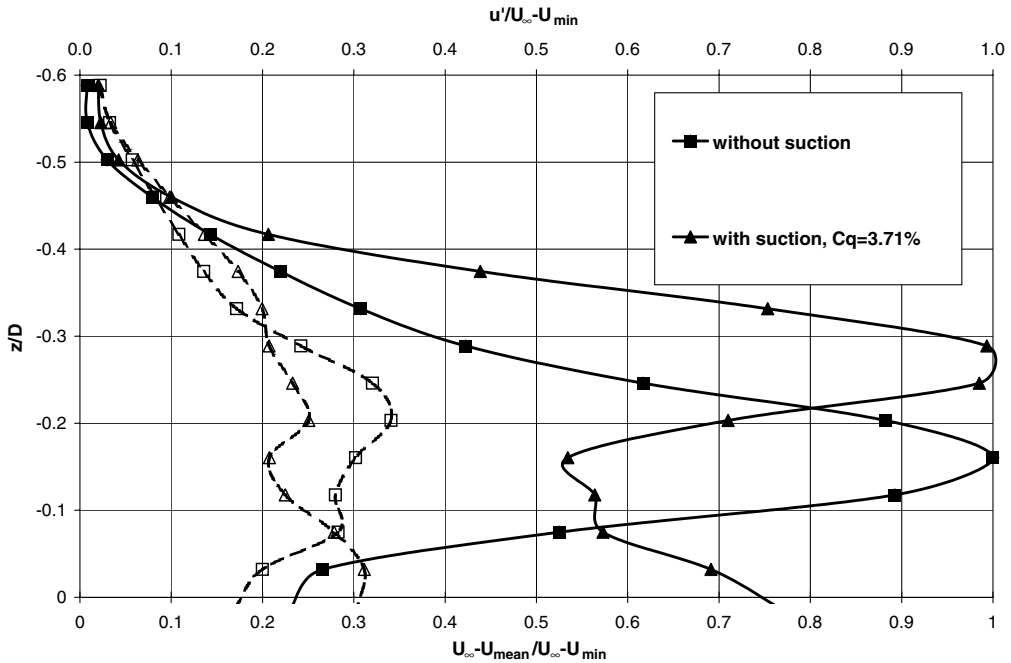

Fig. 14 Normalized wake velocity and turbulence profiles with VGs in positions 2 and 9.

3. Case III: Large Vortex Generators in Positions 3 and 5

Because the asymmetric placement of a single VG had a large influence on the local separation, adding another VG might have amplified the effect.

Figure 17 illustrates the visual effects of the VGs with and without the additional suction ($C_Q = 3.71\%$). Both vortices enhanced the necklace vortex on the right side (looking downstream, Fig. 17). Because of the rotation of the vortices, there was a transport of momentum from the top of the model toward the right side, which maintained the flow attachment over a longer distance. The black arrows mark the separation of these vortices and of the flow over the apex. On the right side, the necklace vortex and the introduced vortices merged together and separated in one area, similar to the flow resulting from a single VG located in position 6. This reflects the velocity and longitudinal turbulence intensity distributions shown in Fig. 18. With two VGs placed upstream of the protuberance, the shift of the wake away from the center was amplified. Compared with case II, which had just one VG, the shift of the main wake peak was doubled. By adding strong suction, the delay of separation in a certain area was reduced, because some of the added vorticity was sucked away or shifted away from the centerline. The flow separated earlier as a result. This increased the momentum deficit around the plane of symmetry and decreased it on the right side. The turbulence intensity distributions (Fig. 18) yield similar results. The area of high turbulence intensity shifted away from the centerline in the absence of suction. The application of suction reduced the turbulence caused by the necklace vortex, but it increased the turbulence level in the central region by advancing the separation location upstream.

V. Experiments on the Hemispherical Protuberance

The preceding experiments were repeated on a hemispherical protuberance and focused on changing the upstream boundary layer and using a single vortex generator upstream of the model. Only the height of the protuberance and the associated base plate were initially changed and, if neither the size nor the location of the VG and the arrangement of the nuts used to thicken the boundary layer was altered, the ratio of the VG height to the height of the protuberance would have been halved.

In addition to the flow visualization with china clay, images in the wake were obtained by introducing smoke into the flow and illuminating the smoke particles with a laser sheet over the entire wake region. A continuous 5 W argon–ion laser and cylindrical lenses were used to create a 4-mm-thick laser light sheet that was perpendicular to the freestream and was located 1 diameter downstream of the model's center. The smoke was introduced into the settling chamber of the wind tunnel, in which a localized layer of smoke was formed close to the tunnel floor. The size of the smoke particles was of the order of 10 μm. A camera was mounted far downstream on the tunnel floor, recording images at a frequency of

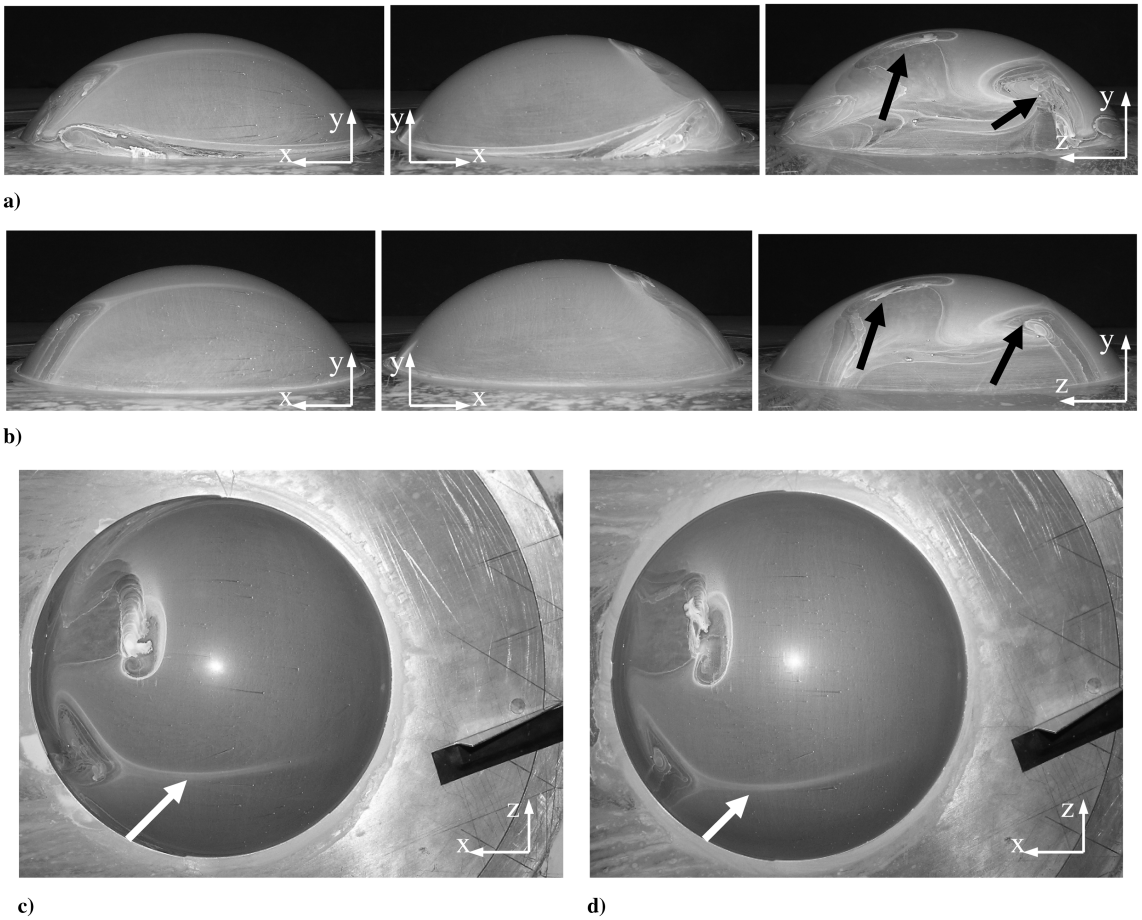

Fig. 15 VG in position 6: a) and c) without suction, b) and d) with suction, $C_Q = 3.71\%$.

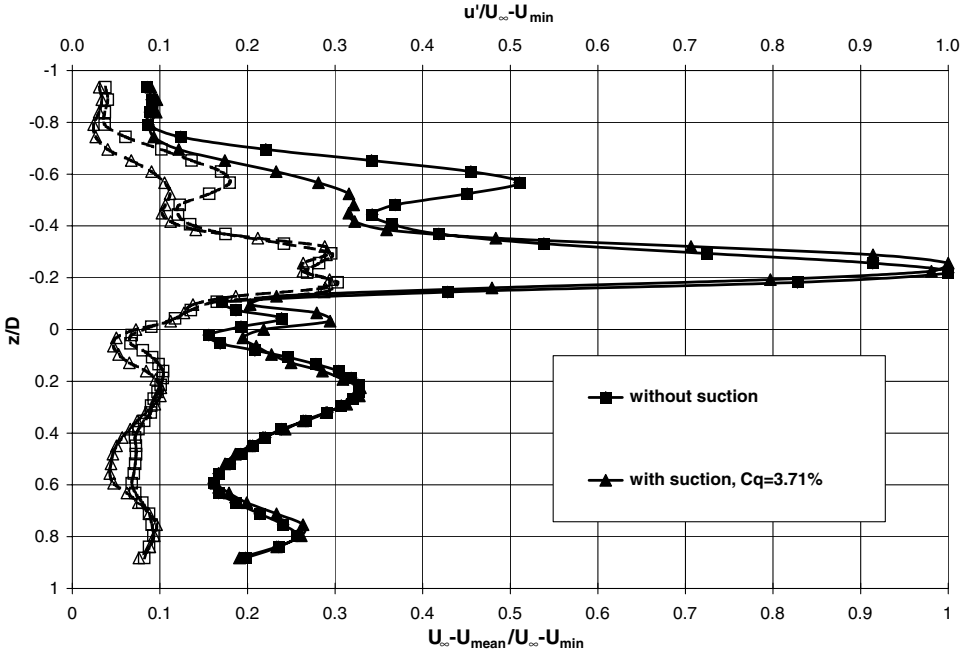

Fig. 16 Normalized wake velocity and turbulence profiles with one VG in position 6.

30 Hz. The freestream velocity used during the smoke visualization was reduced to 12.5 m/s to improve the clarity of the flow structures. However, for the visualizations with china clay, the freestream velocity remained at 20 m/s, defining a Reynolds number of 280,000 based on the diameter of the hemisphere.

A. Visual Results for Baseline Case and Thickened Upstream Boundary Layer

This subsection presents the visual results obtained for the clean baseline case and for the thickened boundary layer upstream of the model. The flow rates for the applied suction were adjusted to obtain

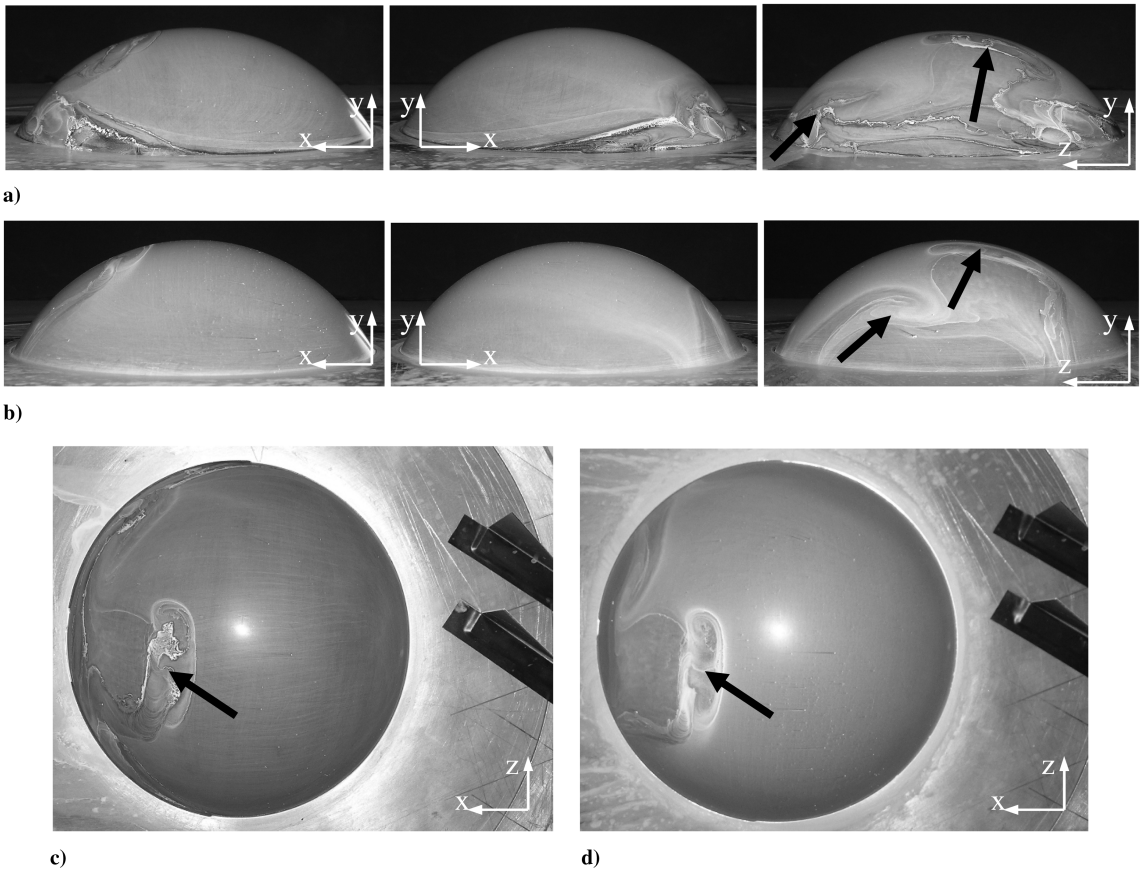

Fig. 17 VGs in positions 3 and 5: a) and c) without suction, b) and d) with suction, $C_Q = 3.71\%$.

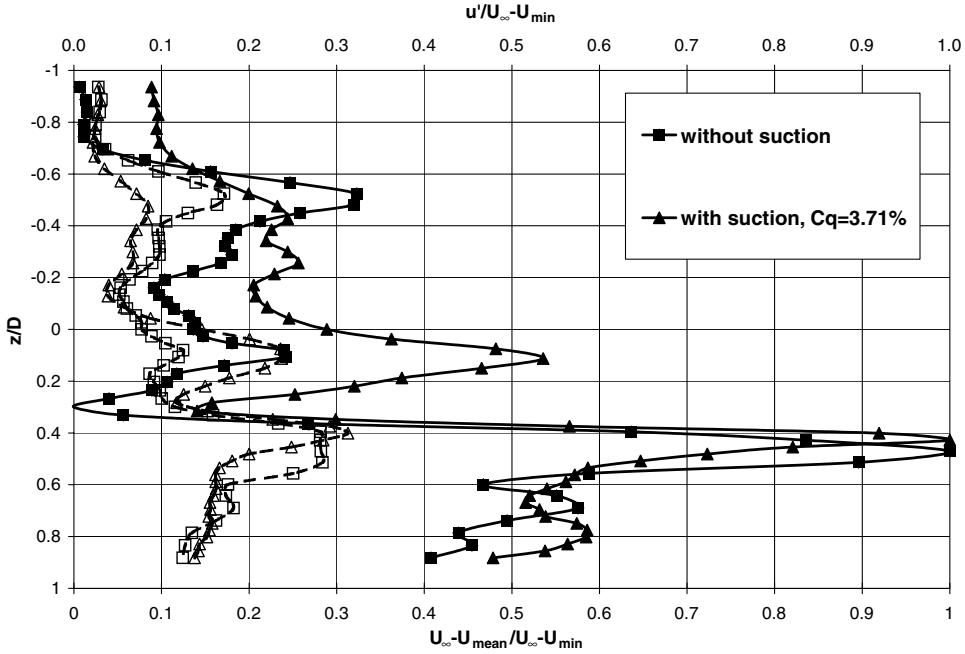

Fig. 18 Normalized wake velocity and turbulence profiles with VGs in positions 3 and 5.

the same C_Q values as for the 120 deg spherical segment because the projected area perpendicular to the freestream was larger for the hemisphere. The smoke visualization for the cases with suction turned out to be ineffective because too much smoke was sucked into the slots and, therefore, not enough particles were left to scatter the light in the plane of view.

The baseline flow using china clay without and with suction is shown in Figs. 19a and 19b, respectively. The same flow patterns as described for the 120 deg spherical segment are visible. The necklace vortex, marked by the white arrows, formed around the base of the hemisphere and was lifted up into the low-pressure zone formed by the separation of the flow from the surface. It almost seemed that the necklace vortex merged with the curved vortex created by the separation from the top of the hemisphere. Traces of the necklace vortex were also evident on the tunnel floor. The flow over the hemisphere immediately separated downstream of the apex.

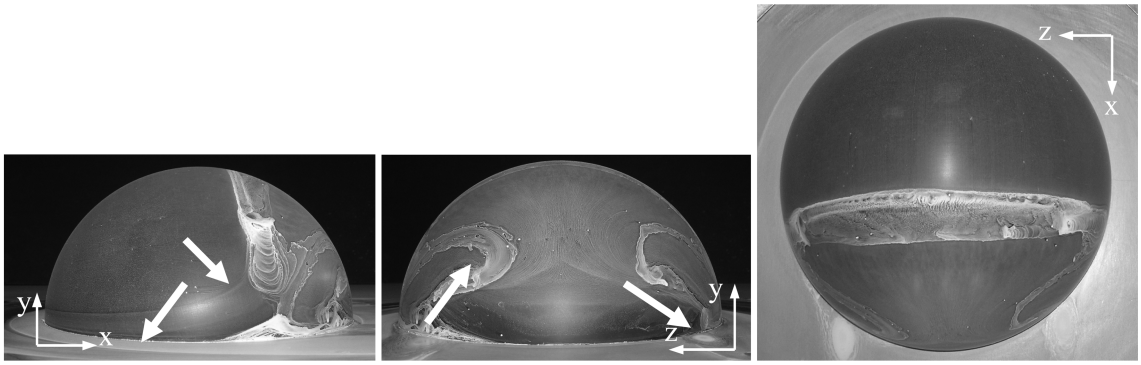

a)

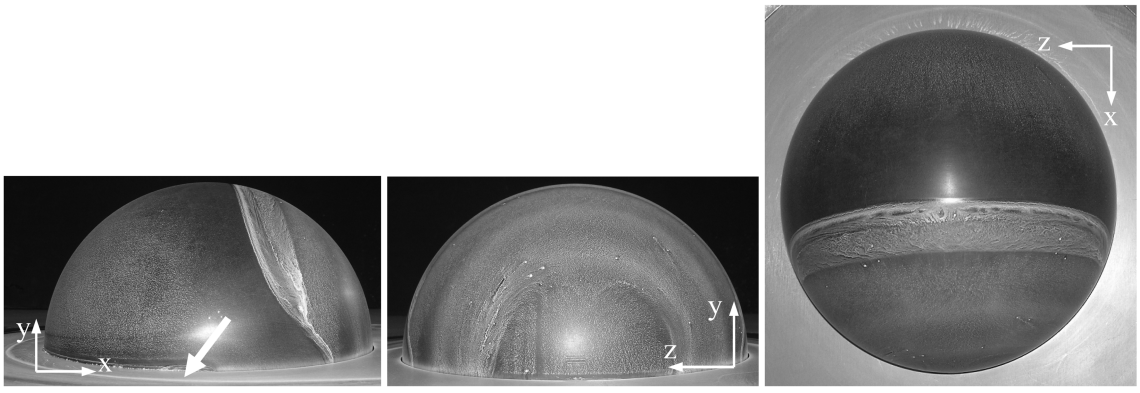

b)

Fig. 19 Baseline: a) without suction, and b) with suction, $C_Q = 3.71\%$.

The separated shear layer interacted with the necklace vortex on the sides of the hemisphere. By applying suction with $C_Q = 3.71\%$, the size of the necklace vortex was reduced, although its traces were still visible on the tunnel floor around the hemisphere. Suction delayed the flow separation along the sides but did not substantially decrease the size of the separated area.

An image of the wake taken 1 diameter downstream of the model's center is shown in Fig. 20. The white dashed line marks the center of the test section. The flow visualization with smoke corroborates the flow patterns seen by using the china clay. The separated flow over the apex created a large recirculation area around the plane of symmetry. The separated necklace vortex evolved downstream close to the tunnel floor next to the recirculation area, but the main region of turbulence appeared to stem from the wake of the body and not from the necklace vortex, as was observed for the 120 deg spherical segment.

Thickening the upstream boundary layer with the nut configuration in case I described in Sec. III generated the results without and with the application of suction shown in Figs. 21a and 21b. It can be observed that the necklace vortex appeared stronger and reached higher into the separated area than in the thin-boundary-layer case. Flow separation was delayed over the apex and also along the sides of the hemisphere (marked by the black arrows). The spanwise size of the shear layer, separated from the apex, was reduced. Some of this improvement was lost with the application of suction because the necklace vortex and its energizing influence were eliminated. However, flow separation along the sides of the hemisphere was delayed.

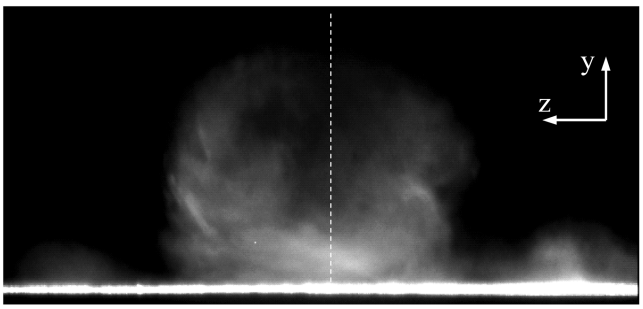

Fig. 20 Wake flow visualization for baseline (no suction, no VGs, unchanged BL).

Figure 22 presents a comparison of the baseline case and the case of a thickened boundary layer in the absence of suction. The delay of flow separation along the plane of symmetry and along the sides is evident. These results support the effective influence of the streamwise vortices that were created in the boundary layer upstream of the model. The different structures in the surface pattern even before separation occurs are partly due to slight variations in the china clay mixtures. Obtaining exactly the same consistency of particle quality and quantity was difficult. However, the small variations in the china clay had no influence on the overall flow pattern, for example, separation location.

B. Visual Results for One Vortex Generator of Different Size in Position 6

The asymmetric placement of a single VG upstream of the model proved to be successful in altering and shifting the wake of the 120 deg spherical segment. This warranted further investigation of a single VG being placed on the plane of symmetry upstream of the model. The visualizations presented in Fig. 23 illustrate the case with one VG in position 6 without suction. The asymmetric influence of the VG is clearly visible in the patterns of the separation area. The vortex created by the VG opposed the necklace vortex on the right side (looking downstream) and enhanced the necklace vortex on the left side, where they merged together at the rear of the hemisphere and separated from its surface. The additional vortex energized the boundary layer over the apex that delayed the separation locally (marked by the black arrow in Fig. 23). Fine tufts of wool were attached to the rear side of the hemisphere to visualize the instantaneous flow patterns. The tuft at the core of the vortex oscillated wildly, showing high separating turbulence, whereas the other tufts mostly represented attached flow. The tuft close to the

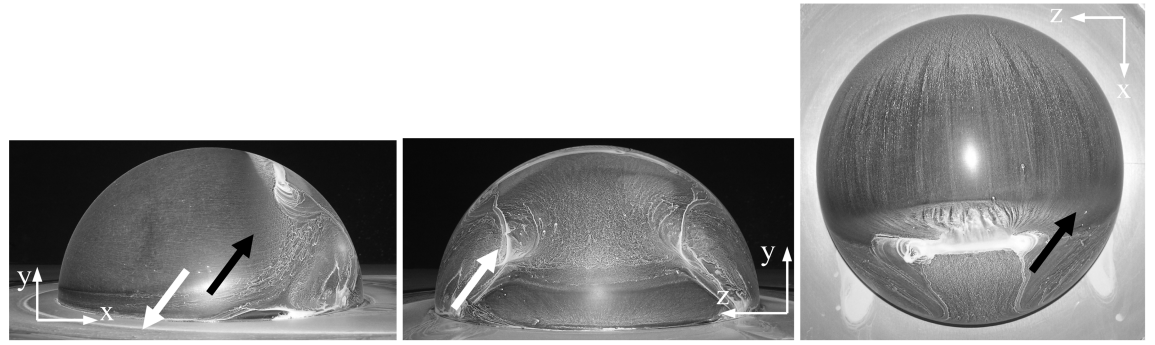

a)

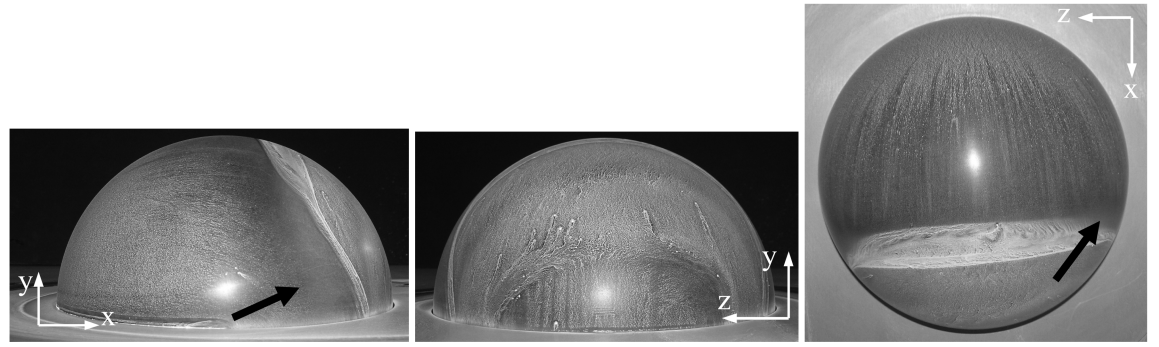

b)

Fig. 21 Thickened BL: a) without suction, b) with suction, $C_Q = 3.71\%$.

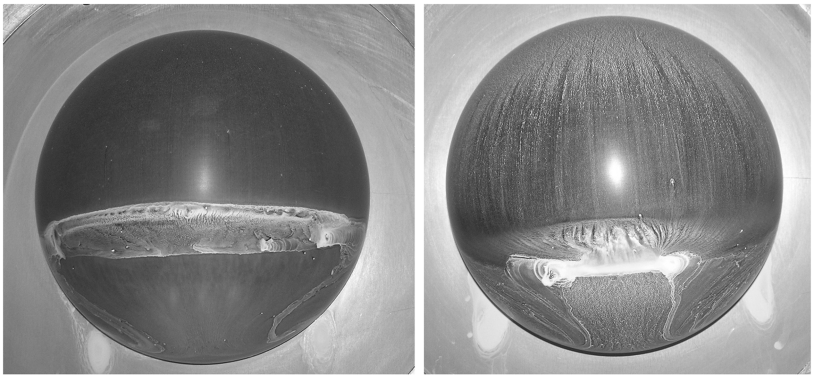

a) b)

Fig. 22 Top views: a) baseline without suction, and b) thickened BL without suction.

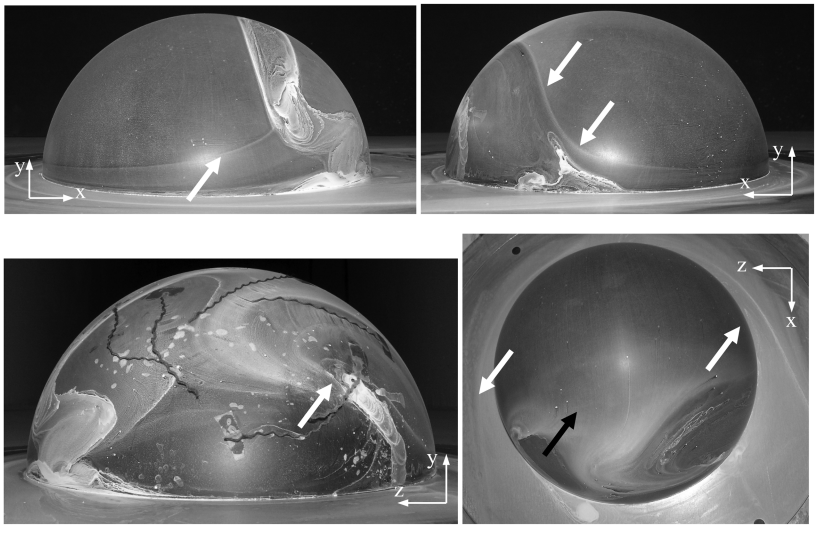

Fig. 23 VG in position 6 without suction.

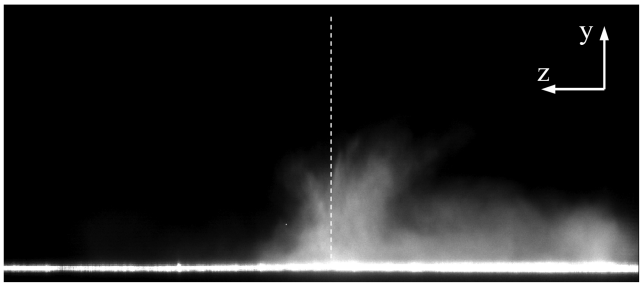

Fig. 24 Wake flow visualization with VG in position 6 without suction.

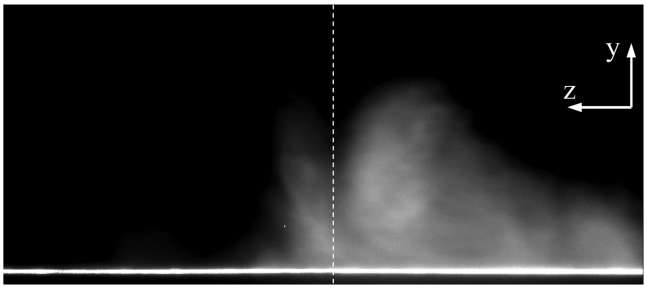

Fig. 26 Wake flow visualization with enlarged VG in position 6 without suction.

tunnel floor showed the typical back flow in the recirculation area, but also the influence of the nearby separating vortex. The circulation patterns of the merged necklace and VG vortex were evident as well. The shift of the entire wake toward the left hand side was apparent from the traces of the necklace vortex on the tunnel floor, which pointed to the left side rather than being symmetrical around the centerline (white arrows).

Figure 24 displays an image of the wake obtained by smoke visualization. The suppression of the necklace vortex on the right side of the hemisphere and the enhanced circulation on the left side are evident. The image has the same scale as the one shown in Fig. 20 and, therefore, reveals the reduction in height of the smoke concentration area resulting from the delayed separation.

The addition of suction reduced the necklace vortex, resulting in a delayed separation along the base of the hemisphere, as already observed. However, the positive influence of the vortices on the flow along the apex was reduced. The separation was still delayed compared with the baseline configuration and the wake was shifted to the left, but these effects appeared to be stronger without the suction.

The strong influence of a single vortex generator raises the question about the importance of the size of the VG. The same experiments were conducted with a VG that was half the original size and twice that size. These different VGs were placed at position 6 with their trailing edge at the same location as the previously used VG. The VG at half the original size, meaning 30 mm in length and 20 mm in height, appeared to have no significant influence on the flow. Figures 25 and 26 display the images obtained by using an enlarged VG (120 mm in length and 80 mm in height) placed in position 6. As observed earlier, the introduced vortex suppressed one side of the necklace vortex and enhanced the other. A major delay in the separation was visible along the centerline at the rear portion of the hemisphere (marked by the black arrow). The footprint of the necklace vortex and the vortex generated by the VG is marked by the white arrows in Fig. 25. The shift of the wake to the left side was again visible from the traces of the necklace vortex on the tunnel floor. Figure 26 illustrates that the right side of the wake (looking downstream) was diminished whereas the left side presented an increased circulation of smoke due to the larger size of the introduced vortex. Although the flow separation was locally delayed, the left side of the wake was increased. However, the localized reduction of the separation area is sufficient when keeping the possible applications in mind.

The application of suction reduced the influence of the larger VG because the necklace vortex was diminished. The missing interaction caused the vortex generated by the VG to penetrate further into the separation area, where it finally separated closer to the centerline than it did without the suction. However, the local delay of separation and the shift of the wake region were still evident.

VI. Conclusions

The long perseverance and strong influence of streamwise vortices in a turbulent boundary layer were examined for flow over a large spherical protuberance of varying height that protruded from the surface. Two protuberances were used; one was a hemisphere and the other was an included arc of 120 deg. Streamwise vortices were created with an array of small hexagonal nuts that were located far upstream of the model. These longitudinal vortices appeared to be stationary over the entire distance between the nuts and the model, eventually interacting with the flow over the spherical protuberance and delaying its separation. With the additional application of suction at the base of the spherical protrusion, flow separation was delayed and the size of the wake was further reduced. Suction eliminated the necklace vortex around the base of the model and, therefore, reduced the turbulence intensity in the periphery of the wake. Tripping the boundary layer along the apex of the model had a minor influence on flow separation at the Reynolds number tested.

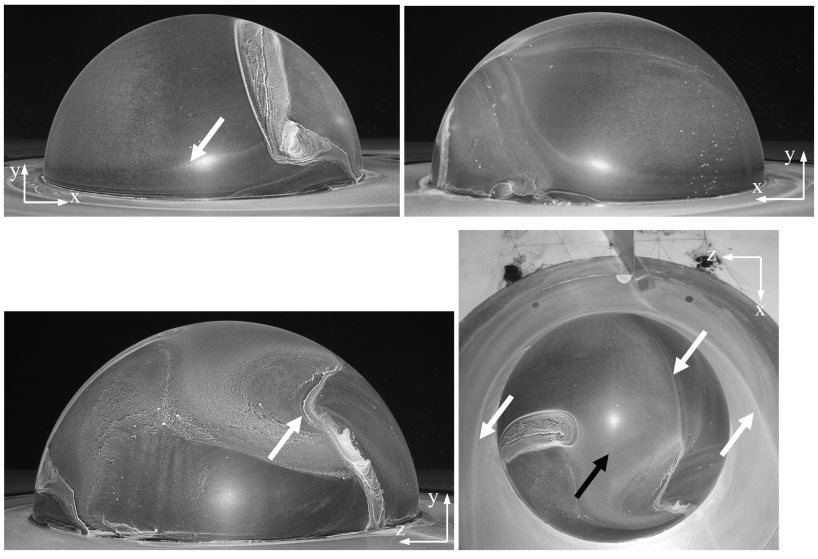

Fig. 25 Enlarged VG in position 6 without suction.

Furthermore, the combination of tripping and thickening of the oncoming boundary layer was not successful, implying that the tripping interfered with and possibly destroyed the streamwise structures in this shear flow. This warranted the use of a small number of large vortex generators placed in a symmetric and asymmetric configuration upstream of the model. The VGs formed vortices that either enhanced or opposed the necklace vortex and delayed flow separation in certain zones of the spherical protuberance. An asymmetric configuration of VGs delayed local flow separation, substantially reducing the turbulence level in the wake. Most of the velocity deficit in the wake and its associated turbulence intensity shifted to either side of the model. The advantage of the large VGs was the strength of the longitudinal vortices that they generated and the orientation of vorticity that they were able to deposit at a location of interest. This suggests that the size, the inclination, and the location of a VG can influence the flow. The flow patterns for the 120 and 180 deg spherical segment appeared to be very similar. For both cases, the same effects were observed but with different intensities. Future research needs to consider comparisons with other setups [10–13] that have used a short cylindrical base under a hemisphere and placed small VGs on the surface of the hemisphere. Additionally, more quantitative investigations of the flow, especially in terms of variables required to reduce the optical aberration, are needed.

Acknowledgment

This investigation was initiated at the suggestion of T. Beutner.

References

[1] Hawthorne, W. R., and Martin, M. E., "The Effect of Density Gradient and Shear on the Flow over a Hemisphere," *Proceedings of the Royal Society of London, Series A: Mathematical and Physical Sciences*, Vol. 232, No. 1189, Oct. 1955, pp. 184–195. doi:10.1098/rspa.1955.0210

[2] Baker, C. J., "The Turbulent Horseshoe Vortex," *Journal of Wind Engineering and Industrial Aerodynamics*, Vol. 6, 1980, pp. 9–23. doi:10.1016/0167-6105(80)90018-5

[3] Toy, N., Moss, W. D., and Savory, E., "Wind Tunnel Studies on a Dome in Turbulent Boundary Layers," *Journal of Wind Engineering and Industrial Aerodynamics*, Vol. 11, 1983, pp. 201–212. doi:10.1016/0167-6105(83)90100-9

[4] Savory, E., and Toy, N., "The Flow Regime in the Turbulent Near Wake of a Hemisphere," *Experiments in Fluids*, Vol. 4, 1986, pp. 181–188. doi:10.1007/BF00717812

[5] Savory, E., and Toy, N., "Hemispheres and Hemisphere-Cylinders in Turbulent Boundary Layers," *Journal of Wind Engineering and Industrial Aerodynamics*, Vol. 23, 1986, pp. 345–364. doi:10.1016/0167-6105(86)90054-1

[6] Savory, E., and Toy, N., "The Separated Shear Layers Associated with Hemispherical Bodies in Turbulent Boundary Layers," *Journal of Wind Engineering and Industrial Aerodynamics*, Vol. 28, 1988, pp. 291–300. doi:10.1016/0167-6105(88)90125-0

[7] Tamai, N., Asaeda, T., and Tanaka, N., "Vortex Structures Around a Hemispheric Hump," *Boundary-Layer Meteorology*, Vol. 39, 1987, pp. 301–314. doi:10.1007/BF00116124

[8] Truman, C. R., and Lee, M. J., "Effects of Organized Turbulence Structures on the Phase Distortion in a Coherent Optical Beam Propagating Through a Turbulent Shear Flow," *Physics of Fluids A*, Vol. 2, No. 5, May 1990, pp. 851–857. doi:10.1063/1.857633

[9] Fitzgerald, E. J., and Jumper, E. J., "The Optical Distortion Mechanism in a Nearly Incompressible Free Shear Layer," *Journal of Fluid Mechanics*, Vol. 512, 2004, pp. 153–189. doi:10.1017/S0022112004009553

[10] Gordeyev, S., Hayden, T. E., and Jumper, E. J., "Aero-Optical and Hot-Wire Measurements of the Flow Around the Hemispherical Turret with a Flat Window," AIAA Paper 2004-2450, June 2004.

[11] Gordeyev, S., Jumper, E. J., Terry, T., and Cain, A. B., "The Optical Environment of a Cylindrical Turret with a Flat Window and the Impact of Passive Control Devices," AIAA Paper 2005-4657, June 2005.

[12] Gordeyev, S., Post, M. L., McLaughlin, T., Ceniceros, J., and Jumper, E. J., "Survey of Optical Environment over Hemisphere-on-Cylinder Turret Using Suite of Wavefront Sensors," AIAA Paper 2006-3074, June 2006.

[13] Cress, J. A., Gordeyev, S., Jumper, E. J., Terry, T., and Cain, A. B., "Similarities and Differences in Aero-Optical Structure over Cylindrical and Hemispherical Turrets with a Flat Window," AIAA Paper 2007-326, Jan. 2007.

[14] Manhart, M., "Vortex Shedding from a Hemisphere in a Turbulent Boundary Layer," *Theoretical and Computational Fluid Dynamics*, Vol. 12, 1998, pp. 1–28. doi:10.1007/s001620050096

[15] Tufo, H. M., Fischer, P. F., Papka, M. E., and Szymanski, M., "Hairpin Vortex Formation, a Case Study for Unsteady Visualization," Department of Energy, Rept. ANL/MCS/CP-99772, July 1999.

[16] Jones, M. I., and Bender, E. E., "CFD-Based Computer Simulation of Optical Turbulence Through Aircraft Flowfields and Wakes," AIAA Paper 2001-2798, June 2001.

[17] Visbal, M. R., Rizzetta, D. P., and Mathew, J., "Large Eddy Simulation of Flow Past a 3-D Bump," AIAA Paper 2007-0917, Jan. 2007.

[18] Schlichting, H., and Gersten, K., "General Properties and Exact Solutions of Boundary-Layer Equations," *Boundary Layer Theory*, 8th ed., Springer–Verlag, New York, 2000, pp. 165–194.

A. Tumin
Associate Editor